Transaction B: Mechanical Engineering
Vol. 17, No. 2, pp. 108–120

SCIENTIA IRANICA

Numerical Modeling of Transient Turbulent Gas Flow in a Pipe Following a Rupture

A. Nouri-Borujerdi[1,*] and M. Ziaei-Rad[1]

Abstract. *The transient flow of a compressible gas generated in a pipeline after an accidental rupture is studied numerically. The numerical simulation is performed by solving the conservation equations of an axisymmetric, transient, viscous, subsonic flow in a circular pipe including the breakpoint. The numerical technique is a combined finite element-finite volume method applied on the unstructured grid. A modified $\kappa - \varepsilon$ model with a two-layer equation for the near wall region and compressibility correction is used to predict the turbulent viscosity. The results show that, for example, after a time period of 0.16 seconds, the pressure at a distance of 61.5 m upstream of the breakpoint reduces about 8%, while this value for the downstream pressure located at the same distance from the rupture is about 14% at the same time. Also, the mass flow rate released from the rupture point will reach 2.4 times its initial value and become constant when the sonic condition occurs at this point after 0.16 seconds. Also, the average pressure of the rupture reduced to 60% of its initial value and remained constant at the same time and under the same condition. The results are compared with available experimental and numerical studies for steady compressible pipe flow.*

Keywords: *Transient compressible flow; Gas pipeline; Numerical modeling; Sudden rupture; Combined finite element-finite volume method.*

INTRODUCTION

In order to evaluate safety and pollution problems due to gas release following a rupture in a pipeline, it is necessary to understand the unsteady fluid dynamics behavior occurring inside the pipeline. Transient gas flow in pipelines has been investigated by several authors.

Osiadacz [1,2] has used a finite difference method for solving a linear model in which inertia forces were neglected. An approximate analytical solution of the problem has been published by Fannelop and Ryhming [3]. Bisgaard et al. [4] developed a one-dimensional finite element method considering the equations of mass, axial momentum and the equation of state to study the unsteady flow of gas in pipelines. They described the results of outflow simulation from a rupture on a horizontal high pressure pipeline and compared the results with actual process data from a full-scale pipeline. Flatt [5] described the results of unsteady compressible flow following a rupture obtained based on the characteristics method. The results were limited to shock-free flows and showed that frictional flows with large values of $4fL/D \approx 1000$ behave very differently from flows without friction. Lang [6] studied the behavior of the gas flow in pipelines following a rupture using a one-dimensional spectral method in both isothermal and adiabatic cases. He found that the flow rate at the breakpoint is nearly the same under isothermal and adiabatic flow conditions. He also indicated that when chock flow occurs at the breakpoint, the space derivative will be singular at this point and a careful approximation of this term in the governing equations is required. Emara-Shabaik et al. [7] evaluated several numerical techniques with respect to their suitability for the real-time monitoring of fluid flow in pipelines assuming one-dimensional isothermal flow with a velocity much less than the acoustic velocity. Pletcher [8] investigated the properties of a preconditioned, coupled, strongly implicit finite-difference scheme for solving a transient compressible flow at low speed. He found that in the start up problem of the unsteady pressure-driven

1. *School of Mechanical Engineering, Sharif University of Technology, Tehran, P.O. Box 11155-9567, Iran.*
*. *Corresponding author. E-mail: anouri@sharif.edu*

Received 21 April 2009; received in revised form 8 September 2009; accepted 10 November 2009

pipe flow, the gas compressibility began to significantly influence the physics of the flow development at quite low Mach numbers. Calay [9] modeled the post-flashing scenario of a jet emanating from a circular orifice due to the release of liquefied gases. A commercial CFD code was used with the models related to turbulence, droplet transport, evaporation, break-up and coalescence. The results showed that whilst a number of features of the experimental results can be reproduced by the CFD model, there are also a number of important shortcomings. Wilkening and Baraldi [10] also employed a commercial code to simulate an accidental gas release from a pipeline as a flow through a small hole between the high-pressure pipeline and the environment. He concluded that because of buoyancy and a higher sonic speed at the release, the hydrogen clouds are farther from the ground level or buildings than in the case of methane clouds. Jo and Ahn [11] proposed a simplified equation of hazard analysis to estimate the hazard area of a pipeline transporting hydrogen. In the event of pipeline failure, the equation relates the diameter, the operating pressure and the length of the pipeline to the size of the affected area. Jo and Ahn in another paper [12] presented a simplified model to estimate the release rate from a hole in a high-pressure gas pipeline. The model included a correction factor accounting for the pressure drop through the pipeline due to the wall friction loss, and the release rate without friction loss. It was found that the model overestimates the release rate slightly and may be a useful tool for estimating the release rate quickly when performing a hazard analysis or risk based management in gas facilities. Luo et al. [13] also proposed a simplified expression for estimating the release rate of hazardous gas from a hole in high-pressure pipelines. The expression included the size of the hole, dimensionless pipeline length, the specific heat ratio of the gas, the frictional force etc. They claimed that taking the first order approximation for the kinetic energy of the flowing liquid resulted in only 7 percent deviation from the theoretical complex equations. Sklavounos and Rigas [14] determined the safety distances around pipelines transmitting liquefied petroleum gas and pressurized natural gas, considering the possible outcomes of an accidental event associated with fuel gas release from pressurized transmission systems. Yuhu et al. [15] presented a mathematical one dimensional model for accidental gas release in long transmission pipelines. They found that, for example, when the initial pipeline pressure is higher than 1.5 MPa, the gas release during sonic flow was more than 90 percent of the total mass of the gas released. Mahgerefteh et al. [16] simulated the fluid dynamics following a rupture in pipeline networks containing multi-component hydrocarbon mixtures. They described a one dimensional numerical model based on the characteristics method. The model accounted for the pipeline bends, branches and couplings and indicated the importance of accounting for pipeline system configuration complexity when simulating such types of failure.

A small amount of experimental research can be found on compressible pipe flow following a rupture. The experimental results of Viola and Leutheusser [17] on unsteady turbulent pipe flow presented a good estimation of turbulence parameters under transient conditions in the pipe flow. Botrosa et al. [18] also measured the flow parameters and decompression wave speeds in a conventional gas mixture and two other rich gas mixtures following the rupture of a high-pressure pipe. They obtained the pressure-time and temperature-time traces using high-frequency response transducers collected at various locations close to the rupture and along the length of the tube.

The major difficulty presented in the previous studies is due to the singularity, which results from the combined effects of friction and choking occurring at the break point. This difficulty is overcome in this study by implementing a combined finite element-finite volume method, following a modified $\kappa - \varepsilon$ model for turbulence properties. Furthermore, a two dimensional analysis is performed around the breakpoint with high Mach numbers, in order to study the effect of radial gradients of flow parameters. Also, the simplifying assumptions of an isothermal and low Mach number flow, often applied in the case of unsteady compressible flows in pipelines, have not been used in this study.

MATHEMATICAL FORMULATION

It is assumed that a compressible flow with a uniform inlet velocity and specified pressure at two ends flows through a pipeline. Suddenly, a rupture is assumed to occur at the middle of the pipeline. Then, an atmospheric pressure is developed at this point (Figure 1).

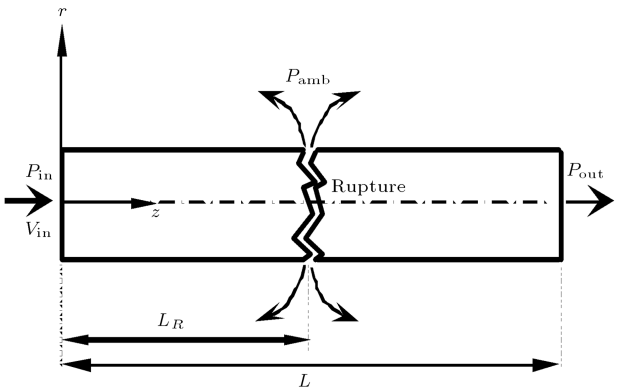

Figure 1. Schematic of a two-dimensional pipe flow with a rupture at the center.

Governing Equations

Under these conditions, it is assumed that a transient two-dimensional compressible turbulent flow is developed in the pipeline. Then, all the governing equations are non-dimensionalized by the following variables:

$$z^* = z/D, \quad u_z^* = u_z/V_0,$$
$$r^* = r/D, \quad u_r^* = u_r/V_0,$$
$$\rho^* = \rho/\rho_0, \quad E^* = E/V_0^2,$$
$$p^* = p/\rho_0 V_0^2, \quad t^* = tV_0/D, \tag{1}$$

where t, ρ, p and E are time, density, static pressure and gas total internal energy, respectively; z and r denote axial and radial directions, respectively; D is the pipe diameter; and V is velocity with u_z and u_r components. The subscript '0' denotes values at a reference state. The superscript '$*$' indicates the dimensionless variables, but for simplicity, we drop this superscript from all equations hereafter. The transport equations for the vector of conservative variables defined by $W = [\rho \quad \rho u_z \quad \rho u_r \quad \rho E \quad \rho\kappa \quad \rho\varepsilon]^T$ will be read in a general form as:

$$\frac{\partial W}{\partial t} + \nabla.F(W) = \nabla.N(W) + S(W), \tag{2}$$

where $F(W)$ and $S(W)$ are the inviscid flux vector and source vector for axi-symmetric flow, respectively. Their components are given by:

$$F_z(W) = \begin{bmatrix} \rho u_z \\ \rho u_z^2 + p \\ \rho u_z u_r \\ (\rho E + p)u_z \\ \rho u_z \kappa \\ \rho u_z \varepsilon \end{bmatrix},$$

$$F_r(W) = \begin{bmatrix} \rho u_r \\ \rho u_z u_r \\ \rho u_r^2 + p \\ (\rho E + p)u_r \\ \rho u_r \kappa \\ \rho u_r \varepsilon \end{bmatrix},$$

$$S(W) = \begin{bmatrix} 0 \\ 0 \\ -\frac{\tau_{\theta\theta}}{r} \\ 0 \\ \mu_t P - \rho\varepsilon_s \\ C_1\rho\kappa P - C_2\rho\frac{\varepsilon_s^2}{\kappa} \end{bmatrix}. \tag{3}$$

The parameter $N(W)$ is the viscous flux vector and its components are given by:

$$N_z(W) = \begin{bmatrix} 0 \\ \tau_{zz} \\ \tau_{zr} \\ k_{\text{tot}}\frac{\partial T}{\partial z} + u_z\tau_{zz} + u_r\tau_{zr} \\ (\mu + \mu_t)\frac{\partial \kappa}{\partial z} \\ (\mu + C_\varepsilon\mu_t)\frac{\partial \varepsilon}{\partial z} \end{bmatrix},$$

$$N_r(W) = \begin{bmatrix} 0 \\ \tau_{rz} \\ \tau_{rr} \\ k_{\text{tot}}\frac{\partial T}{\partial r} + u_z\tau_{rz} + u_r\tau_{rr} \\ (\mu + \mu_t)\frac{\partial \kappa}{\partial r} \\ (\mu + C_\varepsilon\mu_t)\frac{\partial \varepsilon}{\partial r} \end{bmatrix}, \tag{4}$$

where $C_\varepsilon = 0.07$, $C_1 = 0.129$ and $C_2 = 1.83$. T is static temperature and μ and μ_t are gas molecular viscosity and dynamic viscosity of turbulence, respectively. $k_{\text{tot}} = \gamma(\mu/\text{Pr} + \mu_t/\text{Pr}_t)$ is total heat conductivity, where $\text{Pr} = \mu C_P/k$ and $\text{Pr}_t = 0.9$ are Prandtl number and turbulent Prandtl number, respectively. γ and C_p are the specific heat ratio and specific heat capacity of gas, respectively. κ, ε and P denote turbulent kinetic energy, turbulent energy dissipation and production respectively.

The relationship between the pressure and total energy obtained by the equation of state for a perfect gas as well as the stress terms for the tensor components in the governing equations are as follows:

$$p = \rho(\gamma - 1)\left[E - \frac{1}{2}(u_z^2 + u_r^2)\right],$$
$$\tau_{zz} = (\mu + \mu_t)\left[2\frac{\partial u_z}{\partial z} - \frac{2}{3}(\nabla.\vec{V})\right],$$
$$\tau_{rr} = (\mu + \mu_t)\left[2\frac{\partial u_r}{\partial z} - \frac{2}{3}(\nabla.\vec{V})\right],$$
$$\tau_{zr} = (\mu + \mu_t)\left[\frac{\partial u_z}{\partial r} + \frac{\partial u_r}{\partial z}\right],$$
$$\tau_{\theta\theta} = (\mu + \mu_t)\left[2\frac{u_r}{r} - \frac{2}{3}(\nabla.\vec{V})\right]. \tag{5}$$

The dynamic turbulent viscosity is explained by the $\kappa - \varepsilon$ turbulence model, so that:

$$\mu_t = C_\mu\rho\frac{\kappa^2}{\varepsilon}, \tag{6}$$

where $C_\mu = 0.09$.

To prevent an over-prediction of the eddy viscosity by the model, the destruction term is neglected in the turbulent kinetic and dissipation energy equations

and only the shear based components in production term, P, are kept.

$$P = \left(\frac{\partial u_z}{\partial r} + \frac{\partial u_r}{\partial z} \right)^2 . \tag{7}$$

Wilcox [19] proposed the dissipation of the compressibility in terms of the incompressibility as follows:

$$\frac{\varepsilon_s}{\varepsilon} = 1 + H(M_t - M_c) \times \left\{ 1 - \exp\left[-\frac{(M_t - M_c)^2}{\Lambda^2} \right] \right\}, \tag{8}$$

where M is Mach number; $\Lambda = 0.66$; and $H(x)$ is the Heaviside step function defined as:

$$H(x) = \begin{cases} 0 & \text{when} \quad x < 0 \\ 1 & \text{when} \quad x \geq 0 \end{cases} \tag{9}$$

The compressibility correction is made when the turbulent Mach number, $M_t^2 = 2\kappa/a^2$, is more than the cutoff turbulent Mach number, $M_c = 0.25$, where a is the reference speed of sound.

In order to describe low-Reynolds regions close to the solid wall, the classical $\kappa - \varepsilon$ model should be modified. In this case, we use a two-layer approach, where the $\kappa - \varepsilon$ model is introduced by a one-equation model as [20]:

$$\frac{\partial(\rho\kappa)}{\partial t} + \nabla.(\rho V \kappa) - \nabla.[(\mu + \mu_t)\nabla\kappa] = \mu_t . P - \rho \frac{\kappa^{3/2}}{l_\varepsilon}, \tag{10}$$

with the dynamic viscosity of turbulence as:

$$\mu_t = C_\mu \rho l_\mu \sqrt{\kappa}, \tag{11}$$

where the length scales are defined as:

$$l_\varepsilon = C_4 C_\mu^{-3/4} \left[1 - \exp\left(\frac{-y^+}{2C_4 C_\mu^{-3/4}} \right) \right] y,$$

$$l_\mu = C_4 C_\mu^{-3/4} \left[1 - \exp\left(-\frac{y^+}{C_3} \right) \right] y, \tag{12}$$

with $C_3 = 70$ and $C_4 = 0.41$. y^+ is defined by $y^+ = y\sqrt{\kappa\rho\rho_w}/\mu$ where subscript "w" means computed at the closest point of the wall and y is the distance of the current point to this point.

This method enables us to compute the flow from the wall up to $y^+ < 200$ with more computational resources, as a result of a finer mesh size.

Boundary and Initial Conditions

The initial condition is a steady state solution of the pipe flow without any rupture under an adiabatic wall condition. The turbulent kinetic and dissipation energy at the inflow are assumed to be small and set equal to 10^{-5}. The convergence is based on the averaged absolute value of the residual for each conservation equation and is assumed to be less than 10^{-8}. After obtaining the initial condition along the pipe, the solution in the time domain can be found by solving the governing equations with a new boundary condition applied at the rupture point.

Choosing the reference conditions at the inlet of the pipe as known parameters, the set of dimensionless boundary conditions are summarized as follows:

$$\text{inflow}: \begin{cases} \rho(0,r,t) = 1 \\ u_z(0,r,t) = 1 \\ u_r(0,r,t) = 0 \end{cases}$$

$$\text{outflow}: \begin{cases} p\left(\frac{L}{D}, r, t\right) = p_{\text{out}} \\ u_r\left(\frac{L}{D}, r, t\right) = 0 \end{cases}$$

$$\text{wall}: \begin{cases} u_z(z, 0.5, t) = 0 \\ u_r(z, 0.5, t) = 0 \\ q_w(z, 0.5, t) = 0 \end{cases}$$

$$\text{axis}: \begin{cases} \frac{\partial p}{\partial r}(z, 0, t) = 0 \\ u_r(z, 0, t) = 0 \end{cases}$$

$$\text{rupture}: \begin{cases} p\left(\frac{L_R}{D}, 0.5, t > 0\right) = p_{\text{amb}} \\ u_z\left(\frac{L_R}{D}, 0.5, t > 0\right) = 0 \end{cases} \tag{13}$$

where L denotes the pipe length and q_w represents the heat flux on the pipe wall. The subscripts 'R', 'out' and 'amb', respectively, show the rupture point, the outflow and the ambient. It is assumed that the rupture takes place at the time of $t = 0$. The other boundary conditions at the inflow, outflow and breakpoint, rather than those mentioned above, are determined by the characteristic properties convected towards or outwards for subsonic flows with respect to the computational domain, and will be discussed in the numerical technique. The governing partial differential equations together with the boundary conditions, represent a system of equations that will be solved numerically.

NUMERICAL TECHNIQUE

The above governing equations of the transient two-dimensional compressible viscous turbulent flow are solved by the finite volume-Galerkin upwind technique

using the Roe [21] solver for the convective terms and standard Galerkin technique for the viscous terms. The discretization will be carried out on a generally unstructured triangular mesh.

Integral Approximation on Computational Domain

Figure 2 shows grid nodes and discretization of the computational domain, $\Omega = N_t A_t = N_h A_h$, by either triangles (for viscous parts) or hexagonal cells (for inviscid parts) where $A_t(A_h)$ is a triangle (hexagonal) cell area and $N_t(N_h)$ is the number of total triangles (hexagonals). The variables computed on the nodes are denoted by subscript h. If they are the vertices of triangle elements, these nodes are related to the finite element grid. Otherwise, they are related to the control volume in the center of the hexagonal finite volume grid.

The weak finite element formulation of the general equation (Equation 2) without the source term can be written as:

$$\int_{\Omega} \frac{\partial W_h}{\partial t}\phi_h dA + \int_{\Omega} \nabla.\left(F_h - N_h\right)\phi_h dA = 0. \tag{14}$$

In the finite volume calculations, the shape function, ϕ, is equal to one; it is in the finite element computed from the geometry and is used to compute the derivations. Changing the integral of the viscous term, N, using a part by part method and leaving the convective term, F, unchanged with a shape function equal to one the result is:

$$\int_{\Omega} \frac{\partial W_h}{\partial t}\phi_h dA + \int_{\Omega} \nabla.F_h dA + \int_{\Omega} N_h \nabla\phi_h dA - \int_{\partial\Omega} N_h.n\phi_h d\ell = 0, \tag{15}$$

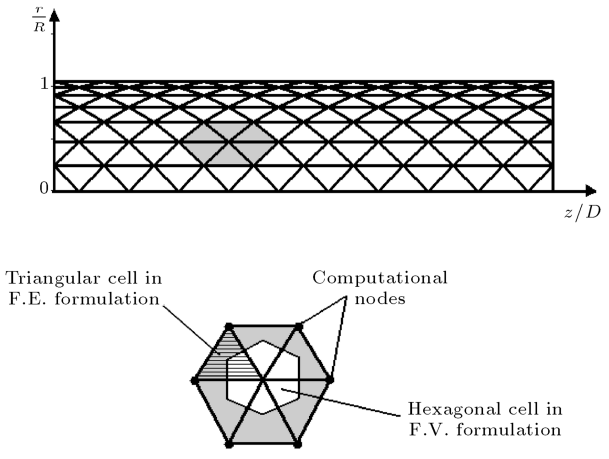

Figure 2. A schematic of computational domain Ω in half part of a pipe.

where $\partial\Omega$ signifies the triangles boundary in the domain.

By using the explicit time integration and introducing the divergence theorem for the convective part, one gets:

$$|A_i|\frac{W^{n+1} - W^n}{\Delta t} + \int_{\partial\ell} F_d.nd\ell = -\int_{\Omega_h} N_h \nabla\phi_h dA + \int_{\partial\Omega} N_h.n\phi_h d\ell, \tag{16}$$

where the superscripts n and $n+1$ denote the old and new time steps, respectively. The index, d, shows that the integral should be computed on the hexagonal edges and the index, $\partial\ell$, denotes the boundary of hexagonal grids. The second term on the right-hand side related to the boundary condition is set to zero herein. These types of convective boundary condition will be applied later by a finite volume formulation. A central scheme is used to compute the viscous term on each cell. For a triangle with vertices denoted by indices 1, 2 and 3, the gradients of the shape functions in z and r directions are defined as:

$$\frac{\partial\phi_i}{\partial z} = r_j - r_k, \quad \frac{\partial\phi_i}{\partial r} = z_k - z_j, \tag{17}$$

where $i, j, k = 1, 2, 3$.

The derivation of each primitive variable appeared in viscous terms, i.e. ρ, u_z and u_r can be computed by the following relation:

$$\frac{\partial\psi}{\partial n} = \psi_1\frac{\partial\phi_1}{\partial n} + \psi_2\frac{\partial\phi_2}{\partial n} + \psi_3\frac{\partial\phi_3}{\partial n}, \tag{18}$$

where $n = z$ or r; $\psi = \rho, u_z$ or u_r.

The mean values of the velocity components on each triangle used in the computation of deformation tensor components and viscous dissipation terms can be obtained as the average of values on the triangle vertices.

$$\bar{u}_n = \frac{1}{3}\left(u_{n,1} + u_{n,2} + u_{n,3}\right), \tag{19}$$

where $n = 2$ or r.

For convective parts, it is supposed that the F vector varies linearly from one side of each triangle to the other. The convection term on the left hand side, therefore, is evaluated by the finite volume Roe method [21] on the control volume surfaces, which are the sides of the hexagonal shape. The flux vector across these planes will be:

$$F = \frac{F_L + F_R}{2} - \frac{1}{2}R|\Lambda|R^{-1}\Delta W, \tag{20}$$

where subscripts 'L' and 'R' denote lower and upper cell indices. F_L and F_R are computed from W_L and W_R, respectively, and $\Delta W = W_R - W_L$. The matrices of eigenvalues, $|\Lambda|$, and eigenvectors, R, of the flux Jacobian matrix, $A = \partial F/\partial W$, for a two-dimensional model, are defined by:

$$\Lambda = \begin{bmatrix} \hat{u}_n - \hat{a} & 0 & 0 & 0 \\ 0 & \hat{u}_n & 0 & 0 \\ 0 & 0 & \hat{u}_n & 0 \\ 0 & 0 & 0 & \hat{u}_n + \hat{a} \end{bmatrix},$$

$$R = \begin{bmatrix} 1 & 0 & 1 & 1 \\ \hat{u}_z - \hat{a}n_z & -\hat{u}_t n_r & \hat{u}_z & \hat{u}_z + \hat{a}n_z \\ \hat{u}_r - \hat{a}n_r & \hat{u}_t n_z & \hat{u}_r & \hat{u}_r + \hat{a}n_r \\ \hat{H} - \hat{u}_n\hat{a} & \hat{u}_t^2 & \hat{V}^2 & \hat{H} + \hat{u}_n\hat{a} \end{bmatrix}, \quad (21)$$

where n_z and n_r are unit normal vectors in axial and radial directions, respectively. $\hat{u}_n = \hat{u}_z n_z + \hat{u}_r n_r$ is the velocity component normal to the hexagonal cell boundaries. $\hat{u}_t = \hat{u}_r n_z - \hat{u}_z n_r$ is the tangential component and $\hat{V}^2 = (\hat{u}_z^2 + \hat{u}_r^2)/2$. The matrices are evaluated by Roe's averages indicated by hat-signs as follows:

$$\hat{\psi} = \frac{\psi_L \rho_L^{1/2} + \psi_R \rho_R^{1/2}}{\rho_L^{1/2} + \rho_R^{1/2}}, \quad (22)$$

where $\psi = u_z$, u_r or H in which H is total enthalpy. Other hat-signed quantities can be computed indirectly from these parameters by use of thermodynamic relations.

The difference between the cylindrical and Cartesian coordinates' terms in the weak form of Navier-Stokes equations comes from the differential area in the integrals ($rdrdz$ replaced by $drdz$). So, we multiply the cell areas, $|A_i|(|\ell_i|)$, and the edge lengths of the computational domain by some radius "r" obtained from the radius of the nodes, r_i. The other modifications come from the additional source terms occurred in the governing equation. Hence, by transferring the additional terms of cylindrical operator to the right hand side of the governing equation in comparison with the Cartesian form, we are able to solve the left hand side of the equation based on a solution of the two dimensional Cartesian coordinate algorithm. The source terms of the model have been taken into account in an explicit way.

The time integration has also been carried out by an explicit scheme and Equation 2 can be rewritten as:

$$\frac{\partial W}{\partial t} = RHS(W), \quad (23)$$

where $RHS(W)$ denotes the right hand side of the equation and contains all convective, viscous and source terms in the equation computed explicitly. The time integration procedure is performed by using the fourth order Runge-Kutta scheme as:

$$W^0 = W^n,$$

$$W^k = W^0 + \alpha_k \Delta t \; RHS(W^{k-1}),$$

$$W^{n+1} = W^4, \quad (24)$$

where the optimum choices for α_k are: $\alpha_k = 0.11$, 0.2766, 0.5, 1.0; for $k = 1$, 2, 3 and 4 [22].

Treatment of the Boundary Conditions

For subsonic flow, the inflow and outflow boundary conditions require two and one specified primitive variables, respectively. These boundaries are treated by a new characteristics technique such that the fluxes are split into positive and negative parts following the sign of the eigenvalues for the Jacobian matrix $A = \partial F/\partial W$ of the convective operator, F [23].

$$\int_{\ell_\infty} F.nd\ell = \int_{\ell_\infty} \left(A^+ W_{\text{in}} + A^- W_{\text{out}}\right).nd\ell, \quad (25)$$

where A^+ and A^- are positive and negative parts of the Jacobian matrix, respectively, and are defined as:

$$A^+ = R|\Lambda^+|R^{-1},$$

$$A^- = R|\Lambda^-|R^{-1}. \quad (26)$$

Λ and R can be easily computed using eigenvalue and eigenvector matrices presented by Equation 21. At the inlet, W_{in} is the interior value and determined by the interior values of the previous iteration. W_{out} is the exterior value and obtained by the flow configuration. In the steady-state subsonic flow, the W_{out} values depend on employing three quantities, which are selected according to the sign of the related eigenvalues. The fourth condition belongs to W_{in} and it is determined by the characteristic property and convected outwards with respect to the computational domain similar to the interior values of W_{in}. At the outlet with a subsonic flow, W_{out} values depend on employing only static pressure and the other three conditions are the characteristic variables convected towards the exterior of the domain, which is set equal to the interior of the previous iteration, similar to W_{in} again. As noted before, the steady state solution of a gas flow under adiabatic conditions is used as an initial condition.

Semi-Unstructured Grid Arrangement over the Computational Domain

An unstructured triangular grid in the z and r directions is employed. However, the position of the nodes in

each direction are arranged to be in one line, similar to structured grid configurations. This enables us to use the algebraic equations to pack the grid point in the desired positions (Figure 2). In order to get enough resolution, the mesh size is fined in the boundary layer region, according to y^+ limitation for a turbulence model. The value y^+ is measured from the pipe wall towards inside. Several mesh sizes were tested to ensure that the results of the numerical solution are mesh size independent. The computational domain consists of 1000 nodes in the z direction clustered near the rupture and 100 non-uniform meshes clustered near the wall in the r direction with an area of $R \times 1000R$. The nodes are packed near the wall, such that there are three nodes within the distance of $y^+ < 10$. The first node is located at $y^+ = 3$, according to the criteria of the two-layer turbulent model. The location of the grid nodes in the r direction is obtained by the following relation:

$$r = \frac{1}{2} + \frac{1}{2}(\beta_r + 1)\frac{\left(\frac{\beta_r+1}{\beta_r-1}\right)^{\eta-1} - 1}{\left(\frac{\beta_r+1}{\beta_r-1}\right)^{\eta} + 1}, \tag{27}$$

where $\beta_r = 1.006$ and $0 \leq \eta < 1$. For the location of the grid nodes in the z direction, also the following algebraic relation is used to pack the grid points in the interior of the domain near the rupture:

$$z = \frac{L_R}{D}\left\{1 + \frac{\sinh\left[\beta_z\left(\xi - A\right)\right]}{\sinh\left(\beta_z A\right)}\right\}, \tag{28}$$

where $0 \leq \xi < 1$ and $\beta_z = 5$ is the clustering parameter. $L_R = L/2$ is the position of the rupture where the clustering is desired. A is defined as:

$$A = \frac{1}{2\beta_z}\ln\left[\frac{1 + \left(e^{\beta_z} - 1\right)\left(L_R/D\right)}{1 + \left(e^{-\beta_z} - 1\right)\left(L_R/D\right)}\right]. \tag{29}$$

Stability and Validation of the Numerical Code

In order to ensure numerical stability, the classical Courant-Friedrichs-Lewy (CFL) stability criterion for the explicit method is utilized in the computations. The following formula is used to compute the local time step for a given node:

$$\Delta t_i = \mathrm{CFL} \times \min\left[\frac{(\Delta x)^2}{(\sqrt{u_z^2 + u_r^2} + a)\Delta x + \frac{2\gamma(\mu+\mu_t)}{\rho\,\mathrm{Pr}}}\right], \tag{30}$$

where Δx is the minimum height of the triangles having the node (i) in common. A small value of CFL = 1 is used in the computation with $\kappa - \varepsilon$ two-equation turbulence modeling. The formula chooses the minimum time step from among those defined according to the CFL definition for inviscid flows together with the time step for viscous parts. For computing the unsteady solution, the minimum local time step is employed.

Two different test cases are used to validate the steady state numerical solution. The first one is the steady state solution of a turbulent flow in the entrance region of a pipe with the inlet Mach number of $M_{\mathrm{in}} = 0.34$ and the Reynolds number of $\mathrm{Re} = \rho_0 V_0 D/\mu = 1.6 \times 10^6$. The uniform wall temperature of the pipe is 330 K. Figure 3 shows the centerline velocity along the pipe under $p_{\mathrm{out}}/p_{\mathrm{in}} = 0.945$ condition. The number of grid points used in this case is 300 × 150. The mesh size is supposed to be uniform in the z direction, but clustered towards to the wall with the smallest mesh size of $y^+ = 1$ and the stretching ratio of $\beta_r = 1.01$. As you can see, there is a good agreement between the velocity of the present work and the experimental data of Ward-Smith [24], while the numerical results of Wang et al. [25] with the Baldwin-Lomax eddy viscosity model overpredict the centerline velocity after $z/D > 25$.

The second test case (Figure 4) is the fully developed axial velocity relative to the bulk velocity across the pipe for the low Mach number of $M_{\mathrm{in}} = 0.01$ and $\mathrm{Re} = 2 \times 10^4$. In this case, the grid resolution is $N_z \times N_r = 81 \times 81$. The figure also reports the numerical results of Xu et al. [26] by using the LES turbulent modeling and the experimental data of Imao and Itoh [27]. The experimental data is obtained by using a single-component Laser-Doppler velocimetry with a good agreement between them.

Figure 5 indicates the skin friction factor of a fully developed adiabatic flow and the mass balance error

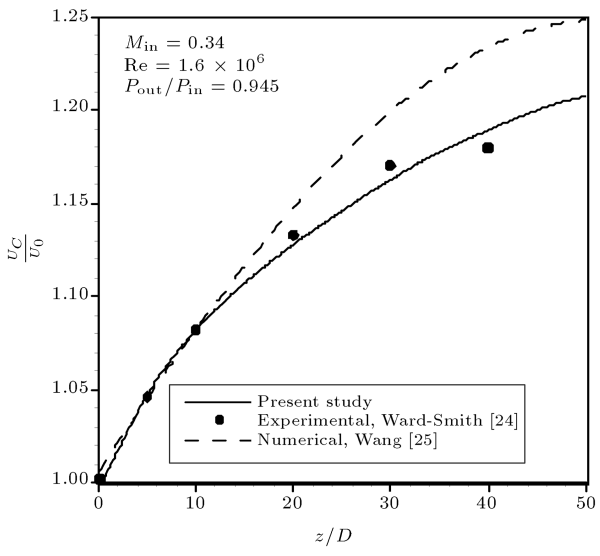

Figure 3. Change in centerline velocity along the pipe for compressible pipe flow.

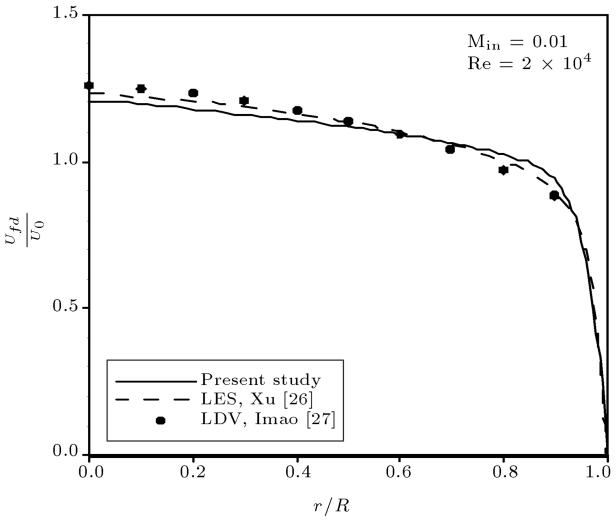

Figure 4. Mean axial velocity profile across the pipe in fully-developed region of nearly incompressible pipe flow.

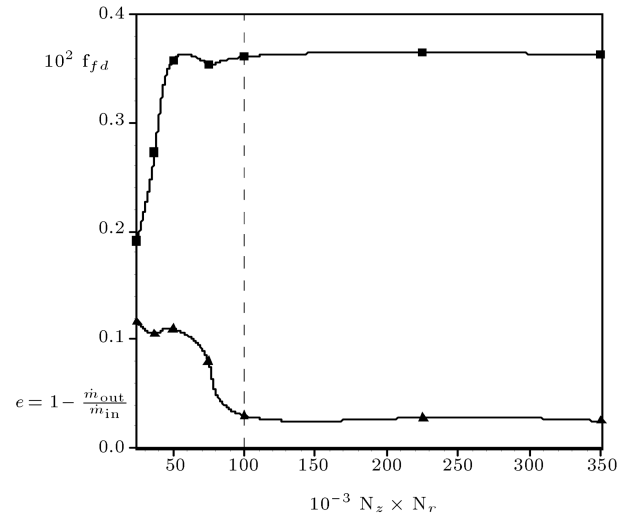

Figure 5. Grid points dependence on skin friction factor and mass balance error.

computed between the inflow and outflow along a pipe with $L/D = 500$. Several grid resolutions are used in the z and r directions clustered at the middle and near the wall, respectively with $\beta_z = 5$ and $\beta_r = 1.006$. The average Reynolds number is $\mathrm{Re} = 9 \times 10^7$ and the inlet Mach number is $M_{\mathrm{in}} = 0.1$. The figure's results show that the friction factor and the mass balance error do not change significantly after node numbers of 1000×100; therefore, these grid points are used as a computational domain.

Parallel Processing

Since computing takes a long time for a long pipeline, it is useful to use parallel processing to divide the computational domain among different processors. Our numerical algorithm is explicit in time and, therefore, parallel algorithms for such an algorithm would be very efficient. For the execution of parallel simulations, a partitioning of the mesh is necessary. Therefore, the computational domain is divided into P subdomains, where P is the number of processors. A symmetric multiprocessing (SMP) machine is used in our parallel computations. With a peak performance of 64 GFLOPS (theoretically), it is possible to have more power in computation by a factor of 5. Some other features of this machine are: 16 core (4x quad-core Xeon E7320, 2.13 GHz, 4 MB L2 cache, 1066 MHz FSB), 96 GB of memory (667 MHz FBD Memory (24x4 GB dual rank DIMM)) and RAID 6 Configuration (4x 300 GB SAS 10.000 RPM, 3.5-inch Hard Drive). The Message Passing Interface (MPI) is implemented to program and run the parallelized code on massively parallel systems. The processors are supposed to be distributed in one dimension along the pipe (Figure 6). In this grid arrangement, the locations of the grid points in the r direction are all on the same straight line for any axial position (see Figure 2). This enables us to define easily the send/receive interfaces between the processors.

Since periodic boundary conditions cannot be used for a compressible pipe flow even in fully developed regions – because the flow properties are varying continuously along the pipe – special options should be specified for the first and the last processors where the inflow and outflow boundary conditions are defined and no send/receive processes are required over these boundaries. On the other hand, in our numerical method, all the nodes (including the boundary nodes) are a part of the computational procedure. Therefore, the grid points for each processor are selected in such a way that there is a one line overlap between grid-points in the interfaces (Figure 6), otherwise, the effects of upstream/downstream cannot be transferred between the processes.

The steady state solution of the compressible flow through a pipe with length $L/D = 500$, $\mathrm{Re} = 9 \times 10^7$ and $M_{\mathrm{in}} = 0.1$ is considered. Such a flow condition and grid configuration will also be used later as an initial condition for unsteady flow analysis from the pipeline

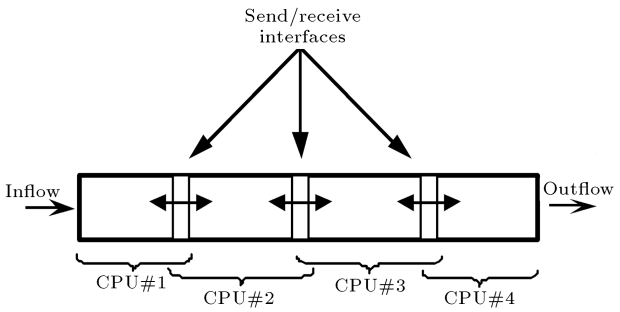

Figure 6. Arrangement of processors along a pipe and data transferring between interfaces.

with a rupture. The grid resolution is 1000 ×100 in the z and r directions, respectively. The location of the grid nodes in the r direction is obtained by Equation 27 with $\beta_r = 1.006$, while the arrangement of grid nodes in the z direction is defined by Equation 28 with $\beta_z = 5$, which leads to grid stretching in the middle of the pipe where the rupture will occur.

Figure 7 shows the running time of a parallel code for this test case versus the number of CPUs. The figure indicates that with the available hardware configuration including 16 processes, the program is running about ten times faster than a single process with an efficiency of about 62.5 percent. After collecting the computational domains from all processes for a steady state solution, a time marching procedure is used to compute the change of flow quantities due to the rupture. This situation is modeled by applying new boundary conditions at the breakpoint. In this case, a special consideration should be taken into account for computation of the time steps. This means that the global time step is obtained by minimizing the values of all processes.

RESULTS AND DISCUSSION

Simulation of Outflow from a Rupture

Gas release has been investigated numerically, following a rupture in the middle of a horizontal pipeline under transient and two-dimensional conditions. The following results are based on perfect gas behavior, i.e. $p = \rho RT$, $R = 287$ j/kg.K and $\gamma = C_p/C_v = 1.4$ through a pipeline with $D = 0.7$ m and $L = 350$ m subjected to an adiabatic condition. The reference conditions of the gas into the pipeline are assumed to be $T_0 = 298$ K, $p_0 = 50$ bar, $M_0 = 0.1$ and $\mu_0 = 1.56 \times 10^{-5}$ N.s/m^2. The outflow pressure of the gas is $p_{\text{out}} = 45$ bar. In this case, the corresponding mass flow rate and the Reynolds number are $\dot{m}_0 = 772$ kg/s and $\text{Re} = \rho_0 V_0 D/\mu_0 = 9 \times 10^7$ respectively. Now, it is assumed that a rupture occurs at the middle of the pipeline, $L_R = L / 2$ with a size of $x_R = 0.4$ and $D = 28$ cm.

Immediately after the rupture incidence, a choking takes place over the cross-section of the pipe and two strong expansion waves start running in two parts of the pipe. After the rupture, it is assumed that the pipeline is divided into two separated parts. The pressure reduction at the breakpoint of the second part causes a reversal flow and the gas flows out from the two ends of this part.

Figures 8 and 9 depict the average pressure and the flow rate profiles as a function of time. A grid

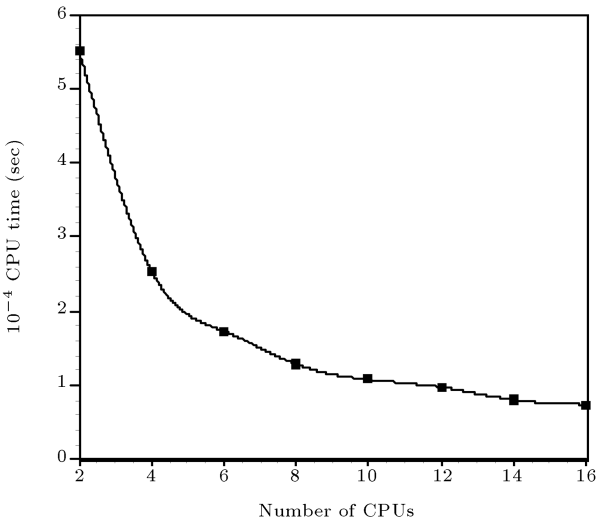

Figure 7. Predicted time for a steady state solution with 1000 × 150 grid points.

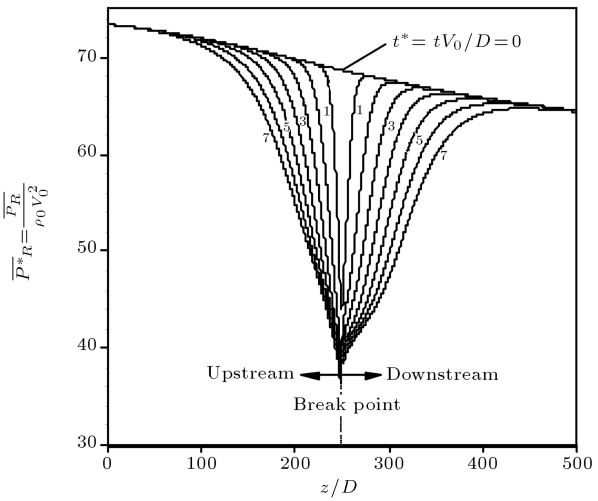

Figure 8. Averaged pressure across at any cross section along the two sections of the pipeline.

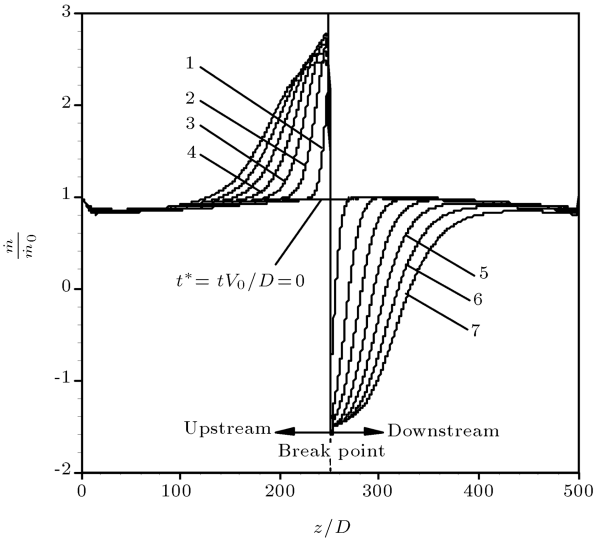

Figure 9. Mass flow rate at any cross section along the two sections of the pipeline.

arrangement of $N_z \times N_r = 1000 \times 100$ is used in the axial and radial directions, respectively. The mesh size is refined in the axial direction with a stretching ratio of $\beta_z = 5$, while it is clustered towards the wall with the smallest mesh size of $y^+ = 1$ and a stretching ratio of $\beta_r = 1.006$ (see Equations 27 and 28). The dimensionless step size for temporal integration is about 10^{-5}. All calculations have been done with a time step sufficiently small so that the results are not affected. At the breakpoint, five grid points are used in the axial direction with the ambient pressure as a boundary condition. Since there is not any available experimental data for the type of problem investigated here in the open literature, and all the previous numerical studies are based on one-dimensional steady state conditions, the validity, accuracy and grid independency of the present results are performed for steady state cases. In addition, a direct comparison between the two-dimensional numerical results of the present work with the one-dimensional numerical results of Lang [6] may be impossible due to the differences between the length of the pipelines and time steps. In the one-dimensional study, the pressure and mass flow rate profiles merge sharply at the breakpoint while in the two-dimensional study, average pressure and the mass flow rate profiles are nearly smooth.

In Figure 8, the 'kink' of the gradient at the breakpoint first was observed by Flatt [5] and, then, was analyzed by Lang [6] and Rhyming [28] as a transition point between the flow regions where inertia and pressure forces govern the flow and the region. It can be seen in this figure that after the rupture, two strong waves start running from the rupture point toward the pipe ends in different directions. The speeds of these two waves are different, since after a time period of $t^* = 8$, the downstream expansion wave reaches the pipe end ($z/D = 500$), while the upstream wave needs more time to reach the pipe inlet ($z/D = 0$).

Some oscillations have been observed in the pressure and Mach number of the breakpoint at early times, which were also reported by Lang [6]. The period of these oscillations at the pipe center are larger than near the pipe wall, since the flow at the pipe center would be less affected by the ambient boundary condition applied on the wall nodes at the rupture. Near the pipe wall at this point ($r^* = 0.5$), the Mach number becomes unity confirming the sonic flow occurs there.

In Figure 9, the mass flow rate on the right side of the rupture (i.e. in the second part of the pipeline) changes from positive to negative values at later stages. It means that the flow direction changes at the leading edge of the second pipe and the gas flows out from both sides of this part.

In hazard analysis, the most important quantity is the flow rate released from the pipe rupture. For times immediately after the break, which is the purpose of this study, the flow behavior will be near adiabatic due to fast transients and the adiabatic thermal boundary condition used here. Figures 10 and 11 show, respectively, how the pressure and outgoing mass flow rate change with time at the breakpoint. As can be found from Figure 10, the pressure at this section reduces sharply and becomes constant after about $t^* = 8$, however, its final value is much more than the ambient pressure, which leads to choked flow at the breakpoint.

Figure 11 also shows that the mass flow rate released from the rupture increases rapidly after the rupture and reaches a constant value when a sonic condition occurs. The mass flow rate consists of the summation of the mass flow from both segments.

Figure 12 shows the variation of pressures with

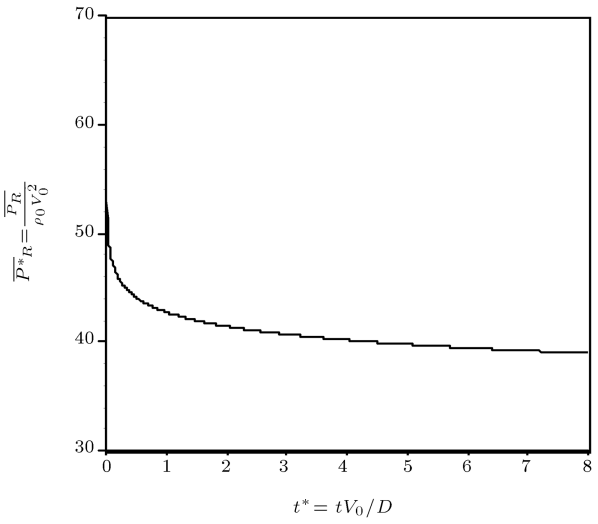

Figure 10. Change in cross-averaged pressure at the rupture with time.

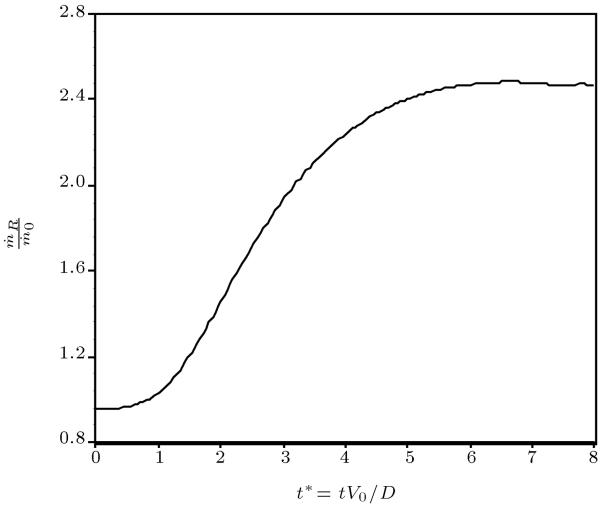

Figure 11. Change in outgoing mass flow rate from the rupture with time.

time in different axial positions along the pipe. The pressure changes slowly at early times after a sudden rupture, and then reduces sharply with time. This figure clearly shows how pressures at the upstream and downstream of the breakpoint, close to or far from this point, will be affected by the rupture. From this figure, it can be found that the reduction in downstream pressures in the position between the outflow and the breakpoint are more than the upstream ones; a result which can also be realized from Figure 8. It can be calculated, for example, that the cross-averaged pressure at the position of $z/L = 0.325$ (equivalent to -61.5 m from the breakpoint) reduced about 8% after a time period of 0.16 seconds, while this value for the downstream pressure positioned at $z/L = 0.675$ (equivalent to $+61.5$ m from the breakpoint) is about 14% at the same time.

Figure 13 also shows the change in mass flow rate at different axial positions along the pipeline. This figure also shows how and when the mass flow rate at different positions of the pipe will be affected by the rupture. As a case, within a time period of 0.04 sec ($t^* = 2$), the outflow rate of the mass in position $z/L = 0.54$ (which is located $+14.7$ m from the rupture) reduces continuously until reaching zero, then, the direction of the flow in this section is changed and after $t = 0.16$ sec it becomes constant while flowing in a reverse direction toward the breakpoint.

CONCLUSIONS

A two-dimensional unsteady turbulent compressible high pressure gas flow with a rupture at its center is studied numerically. The objective of this research was to obtain the time traces of the flow properties exhausted from the rupture, considering the effects of both axial and radial gradients around the rupture. A computer code was developed by a mixed finite element – finite volume formulation for an unstructured grid. Generation of the computational grid nodes was also carried out by a subroutine developed as part of the code. The turbulence modeling is based on the $\kappa - \varepsilon$ model, followed by a two layer technique near the wall. Parallel computing was also implemented to reduce the CPU time, since applying small time steps, which is necessary to prevent the effects of numerical errors on time varying parameters leads to very large CPU time.

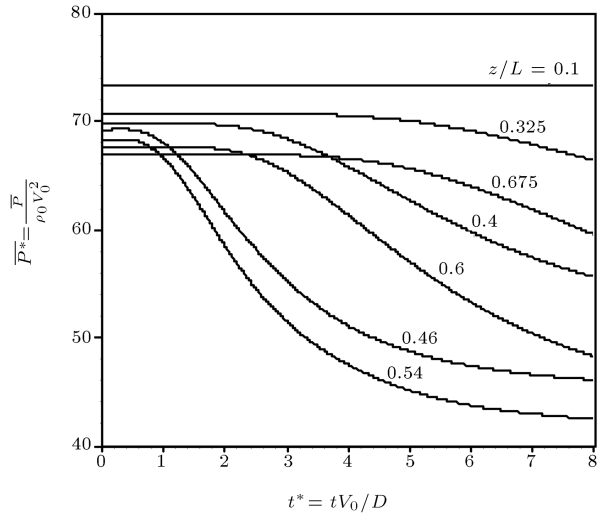

Figure 12. Cross-averaged pressure versus time in different axial positions.

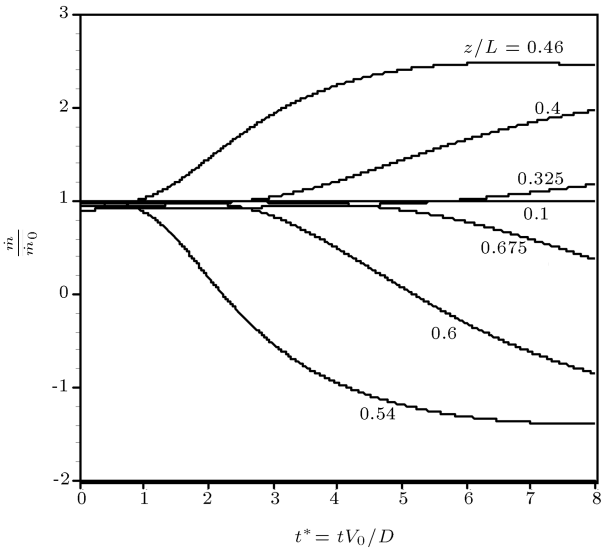

Figure 13. Cross-averaged mass flow rate in different axial positions.

The results show that the present numerical scheme is stable, accurate and efficient enough to solve the problem of the gas flow in a pipeline following a sudden rupture. Also, by using two-dimensional analysis, it is not necessary to model the flow after the choked exit by the quasi steady-state flow through a nozzle. In addition, the singularity problem, which occurs at the breakpoint in a one-dimensional analysis and which affects numerical accuracy will not occur in the proposed technique. Two-dimensional modeling of the rupture problem allows us to take into account the interaction of flows from each segment of the pipe at the breakpoint. From the results, it is observed that the downstream pressure would be more affected by the rupture. The results also indicate that, for example, after a time period of 0.16 seconds, the pressure at a distance of 61.5 m upstream of the breakpoint reduces about 8% while this value for the downstream pressure positioned at the same distance is about 14% at the same time. The mass flow rate released from the rupture will reach 2.4 times its initial value and becomes constant when the sonic condition happens at this point after 0.16 seconds. At the same time and under the same conditions, the average pressure of the

rupture reduced to 60% of its initial value and remained constant at this value.

NOMENCLATURE

A	Jacobian matrix, clustering coefficient
a	sound speed
C	constant
D	pipe diameter
E	total internal energy
F	vector of inviscid flux
f	friction factor
H	total enthalpy, Heaviside step function
k	number of triangles, thermal conductivity
L	pipe length
l	length scale
M	Mach number, $V/\sqrt{\gamma RT}$
$\dot{m}$	mass flow rate
N	vector of viscous flux, count
n	unit normal vector
Pr	Prandtl, $\mu C_P/k$
P	production
p	static pressure
R	pipe radius, matrix of eigenvectors, gas constant
Re	Reynolds number, $\rho \bar{V} D/\mu$
r	radial direction
S	source term
T	temperature
t	time
u	velocity component
V	velocity vector
W	vector of conservative variables
y	distance measured from wall inwards
z	axial direction

Greek Letters

α	Range-Kutta method coefficient
β	clustering parameter
Δ	difference
ε	turbulent dissipation energy
ϕ	shape function
γ	specific heat ratio
κ	turbulent kinetic energy
Λ	eigenvalue matrix, compressibility correction
μ	dynamic viscosity
ρ	density
τ	shear stress
Ω	computational domain
ψ	general function

Subscripts

amb	ambient
c	cut off
fd	fully developed
h	discretized domain, hexagonal cell
in	inlet
i, j, k	direction, counter
L	lower cell index
n	normal to control volume boundary
out	outlet
R	rupture, upper cell index
r, θ, z	cylindrical coordinates
t	turbulent, tangential, triangular cell
tot	total
w	wall
0	reference

Superscripts

$1, 2, 3$	indices for triangle vertices
k	Range-Kutta method steps
n	time step iteration
$\wedge$	Roe-average quantity
$+/-$	positive/negative eigenvalues
$-$	mean value

REFERENCES

1. Osiadacz, A. "Optimal numerical method for simulating flow of gas in pipelines", *Int. J. Num. Methods Fluids*, **3**(2), pp. 125-135 (1983).
2. Osiadacz., A. "Simulation of transient gas flows in networks", *Int. J. Num. Methods Fluids*, **4**(1), pp. 13-24 (1984).
3. Fannelop, T.K. and Ryhming, I.L. "Massive release of gas from long pipelines", *AIAA Journal of Energy*, **6**(2), pp. 132-140 (1982).
4. Bisgaard, C., Sorensen, H.H. and Spangenberg, S. "A finite element method for transient compressible flow in pipelines", *Int. J. Num. Methods Fluids*, **7**(3), pp. 291-303 (1987).
5. Flatt, R. "Unsteady compressible flow in long pipelines following a rupture", *Int. J. Numerical Methods Fluids*, **6**(2), pp. 83-100 (1986).
6. Lang, E. "Gas flow in pipelines following a rupture computed by a spectral method", *J. Appl. Math. Phys.*, **42**(2), pp. 183-197 (1991).

7. Emara-Shabaik, H.E., Khulief, Y.A. and Hussaini, I. "Simulation of transient flow in pipelines for computer-based operations monitoring", *Int. J. Num. Methods Fluids*, **44**(3), pp. 257-275 (2004).
8. Pletcher, R.H. "On solving the compressible Navier-Stokes equations for unsteady flows at very low Mach numbers", Report AIAA-93-3368 (1993).
9. Calay, R.K. and Holdo, A.E. "Modelling the dispersion of flashing jets using CFD", *J. Hazardous Materials*, **154**(1-3), pp. 1198-1209 (2008).
10. Wilkening, H. and Baraldi, D. "CFD modelling of accidental hydrogen release from pipelines", *Int. J. Hydrogen Energy*, **32**(13), pp. 2206-2215 (2007).
11. Jo, Y.D. and Ahn, B.J. "Analysis of hazard area associated with hydrogen gas transmission pipelines", *Int. J. Hydrogen Energy*, **31**(14), pp. 2122-2130 (2006).
12. Jo, Y.D. and Ahn, B.J. "A simple model for the release rate of hazardous gas from a hole on high-pressure pipelines", *J. Hazardous Materials*, **97**(1-3), pp. 31-46 (2003).
13. Luo, J.H., Zheng, M., Zhao, X.W., Huo, C.Y. and Yang, L. "Simplified expression for estimating release rate of hazardous gas from a hole on high-pressure pipelines", *J. Loss Prevention in the Process Industries*, **19**(4), pp. 362-366 (2006).
14. Sklavounos, S. and Rigas, F. "Estimation of safety distances in the vicinity of fuel gas pipelines", *J. Loss Prevention in the Process Industries*, **19**(1), pp. 24-31 (2006).
15. Yuhu, D., Huilin, G., Jing'en, Z. and Yaorong, F. "Mathematical modeling of gas release through oles in pipelines", *Chemical Engineering Journal*, **92**(1-3), pp. 237-241 (2003).
16. Mahgerefteh, H., Oke, A. and Atti, O. "Modelling outflow following rupture in pipeline networks", *Chemical Engineering Science*, **61**(6), pp. 1811-1818 (2006).
17. Viola, J.P. and Leutheusser, H.J. "Experiments on unsteady turbulent pipe flow", *J. Engineering Mechanics (ASCE)*, **130**(2), pp. 240-244 (2004).
18. Botrosa, K.K., Geerligsa, J., Zhoub, J. and Gloverb, A. "Measurements of flow parameters and decompression wave speed following rupture of rich gas pipelines, and comparison with GASDECOM", *Int. J. Pressure Vessels and Piping*, **84**(6), pp. 358-367 (2007).
19. Wilcox, D.C. "Dilatation-dissipation corrections for advanced turbulence models", *AIAA Journal*, **30**(11), pp. 2639-2646 (1992).
20. Wolfstein, M. "The velocity and temperature distribution of one-dimensional flow with turbulence augmentation and pressure gradient", *Int. J. of Heat and Mass Transfer*, **12**, pp. 301-318 (1969).
21. Roe, P.L. "Characteristic-based schemes for the Euler equations", *Annual Review of Fluid Mechanics*, **18**, pp. 337-365 (1986).
22. Lallemand, M.H. "Schemas decentres multigrilles pour la resolution des equations D'Euler en elements finis", Thesis, University of Provence Saint Charles (1988).
23. Steger, J. and Warming, R.F. "Flux vector splitting for the inviscid gas dynamic with applications to finite-difference methods", *J. Computational Physics*, **40**, pp. 263-293 (1981).
24. Ward-Smith, A.J., *Internal Fluid Flow*, Clarendon Press, Oxford, UK, p. 247 (1980).
25. Wang, C.R., Towne, C.E., Hippensteele, S.A. and Poinsatte, P.E. "Heat transfer computations of internal duct flows with combined hydraulic and thermal developing length", Report NASA TM-107450 (May 1997).
26. Xu, X., Lee, J.S. and Pletcher, R.H. "A compressible finite volume formulation for large eddy simulation of turbulent pipe flows at low mach number in cartesian coordinates", *J. Computational Physics*, **203**(1), pp. 22-48 (2005).
27. Imao, S. and Itoh, M. "Turbulent characteristics of the flow in an axially rotating pipe", *Int. J. Heat and Fluid Flow*, **17**(5), pp. 444-451 (1996).
28. Rhyhming, I.L. "On the expansion wave problem in a long pipe with wall friction", *J. Appl. Math. Phys.*, **38**(3), pp. 378-390 (1987).

BIOGRAPHIES

A. Nouri received his PhD degree in mechanical engineering in 1985 at the University of Wisconsin at Madison, USA. He is now professor of mechanical engineering at Sharif University of Technology in Tehran, where he teaches courses at the 'thermal/fluids sciences group' of the mechanical engineering department. His teaching focuses on heat transfer, computational fluid dynamics and two-phase flows, including boiling and condensation, at undergraduate and graduate levels. His current research programs include numerical simulation of compressible turbulent flows, two-phase flow and porous media. Professor Nouri has also published more than 100 articles in international journals and conference papers.

Masoud Ziaei-Rad received his BS degree from Yazd University in Iran and his MS degree from Ferdowsi University of Mashhad, in thermal-fluid science. He earned his Ph.D. degree from Sharif University of Technology, Tehran, in 2009. Dr Ziaei-Rad visited the 'Institute of Turbomachinary and Fluid Dynamics' (TFD) at Leibniz University of Hannover, Germany, as a guest researcher in 2008 and is a faculty member of the school of engineering, mechanical engineering department, in Shahrekord University, Iran. Dr Ziaei teaches heat transfer, fluid mechanics and heat exchanger design, as well as boundary layer theory courses. His current research is compressible turbulent flows with heat transfer in nano-scale structures, and 3D numerical simulation.